This is a repository copy of *Insights into the electrochemical reduction products and processes in silica anodes for next-generation lithium-ion batteries*.

White Rose Research Online URL for this paper:
http://eprints.whiterose.ac.uk/164245/

Version: Published Version

**Article:**

FULL PAPER

ADVANCED
ENERGY
MATERIALS
www.advenergymat.d

Check for
updates

# Insights into the Electrochemical Reduction Products and Processes in Silica Anodes for Next-Generation Lithium-Ion Batteries

*Jake E. Entwistle, Samuel G. Booth, Dean S. Keeble, Faisal Ayub, Maximilian Yan, Serena A. Corr, Denis J. Cumming,\* and Siddharth V. Patwardhan\**

The use of silica as a lithium-ion battery anode material requires a pre-treatment step to induce electrochemical activity. The partially reversible electrochemical reduction reaction between silica and lithium has been postulated to produce silicon, which can subsequently reversibly react with lithium, providing stable capacities higher than graphite materials. Up to now, the electrochemical reduction pathway and the nature of the products were unknown, thereby hampering the design, optimization, and wider uptake of silica-based anodes. Here, the electrochemical reduction pathway is uncovered and, for the first time, elemental silicon is identified as a reduction product. These insights, gleaned from analysis of the current response and capacity increase during reduction, conclusively demonstrated that silica must be reduced to introduce reversible capacity and the highest capacities of 600 mAh g$^{-1}$ are achieved by using a constant load discharge at elevated temperature. Characterization via total scattering X-ray pair distribution function analysis reveal the reduction products are amorphous in nature, highlighting the need for local structural methods to uncover vital information often inaccessible by traditional diffraction. These insights contribute toward understanding the electrochemical reduction of silica and can inform the development of pretreatment processes to enable their incorporation into next-generation lithium-ion batteries.

Dr. J. E. Entwistle, Dr. S. G. Booth, F. Ayub, M. Yan, Prof. S. A. Corr,
Dr. D. J. Cumming, Prof. S. V. Patwardhan
Department of Chemical and Biological Engineering
The University of Sheffield
Mappin Street, Sheffield S1 3JD, UK
E-mail: d.cumming@sheffield.ac.uk; s.patwardhan@sheffield.ac.uk
Dr. D. S. Keeble
Diamond Light Source
Harwell Campus
Oxfordshire X11 0DE, UK
Prof. S. A. Corr
Department of Materials Science and Engineering
The University of Sheffield
Mappin Street, Sheffield S1 3JD, UK

The ORCID identification number(s) for the author(s) of this article can be found under https://doi.org/10.1002/aenm.202001826.

## 1. Introduction

Increased energy and power densities, in combination with lower cost active materials, will accelerate the integration of lithium ion batteries (LIBs) into large-scale renewable storage and the electrification of transport.[1] Challenges to be overcome include, but are not limited to, the discovery and optimization of advanced anode materials. One such possibility is the use of silica, once thought to be electrochemically inactive toward lithium due to low ion diffusivity and further hampered by its electronically insulating nature.[4] However, recent work[2] has demonstrated that silica can react with lithium in a partially reversible process, with prolonged exposure to low voltages (<200 mV vs Li/Li$^+$) promoting electrochemical activity. These observations, in addition to its high natural abundance, low cost, and well-explored synthesis, make silica an attractive, low-cost and sustainable prospect for anode applications although an understanding of fundamental mechanisms behind this performance remains poorly understood.[3] Further, the presence of varying amounts of silica within commercial silicon anodes is common[2] and fundamental insights that inform the nature of reduction products are critical for understanding long-duration stability and the behavior of silica in these next-generation anodes.

Up to now, the majority of reports have detailed only the low first cycle coulombic efficiencies for silica, which indicate significant irreversible processes are taking place (see Table S1, Supporting Information). Interestingly, Lepoivre et al. have recently demonstrated the electrochemical reduction of Stöber silica particles (size ≈200 nm), showing that an initial pretreatment step of prolonged potentiostatic discharge (PSD) of up to 250 h was required before reversible reactions were observed for the silica particles. In that study, a capacity of 400 mAh g$^{-1}$ was achieved and showed good stability over 150 cycles.[2] This necessity of an electrochemical reduction step prior to reversible capacity performance is intrinsically linked to low coulombic efficiencies in the first cycle. This provides an

engineering challenge to the wider uptake of silica as an active material for commercial full cells, where a limited lithium inventory requires initial efficiencies to be >90%. It is therefore likely that such electrodes will require additional electrochemical reduction processing before construction into full cells.[5]

The key challenges, therefore, in overcoming the bottleneck to silica anode exploitation, are in understanding this electrochemical reduction process, optimizing the reduction reaction conditions and times, and obtaining anode materials with sustained high capacities over prolonged cycling regimes. Engineering the direct use of silica in LIBs can provide significant economic benefits. Currently, the nature of the reduction reaction products between lithium and silica is a matter of debate.[6–9] The fully reduced silicon is commonly ascribed as the electrochemically active species, primarily due to the similarities observed in the voltage profiles observed of these electrodes. However, to date no direct characterization of the reduced species has been achieved owing to challenges with in situ measurements and the likely amorphous nature of the reduced species. Traditional techniques such as X-ray diffraction (XRD),[6] NMR,[7] X-ray photoelectron spectroscopy (XPS),[7,8] high-resolution transmission electron microscopy (HRTEM),[7] and selected area electron diffraction (SAED)[7,9] have proved inconclusive as to the nature of $Li_xSi_yO_z$ and $Li_yO_z$ species formed during silica reduction and have not shown the presence of the postulated silicon product.

Here, we present a new methodology for understanding the electrochemical reduction process by investigating capacity increase and current flow during the reduction reaction. We have applied bioinspired silica (BIS) as a new silica anode material, whose benefits include commercial viability (economic, scalability, and sustainability) and diversity in porous morphologies compared to Stöber silica and mesoporous silica.[10–12] In addition to this, BIS has achieved higher capacity of 600 mAh $g^{-1}$ and in a short electrochemical reduction time of 13 h. The determination of likely-amorphous reduction products, where long-range order does not persist, is made possible by the application of X-ray total scattering methods. Such insights are vital to uncovering the underpinning mechanisms behind electrochemical reduction reactions, paving the way for direct use of silica in LIBs

## 2. Experimental Section

### 2.1. Silica Synthesis

For BIS preparation, 31.82 g (0.15 moles) sodium metasilicate (Sigma-Aldrich) was dissolved in 4650 mL deionized water, inside a 5 L Radley's reactor.[13] The solution was brought up to a mixing speed of 450 rpm, after which 5.80 g (0.025 moles) pentaethylene hexamine (PEHA) (Sigma-Aldrich) was added to the solution. Hydrochloric acid (350 mL, 1 M) (Sigma-Aldrich) was added to the reaction mixture and the pH was monitored using a pH probe. Using a micropipette, additional HCl was added to adjust the pH to 7.00 ± 0.05 within 2 min. After 5 min of reaction time, the reaction solution was collected from the bottom of the reactor. Vacuum filtration was used to remove unreacted species and separate silica with at least two washes

with deionized water. Oven drying at 120 °C for 24 h followed by drying under vacuum at 120 °C for 24 h was used to completely dry the BIS. Finally, the BIS was calcined at 550 °C in a tube furnace (Carbolite) under air for 3 h to remove any organic residues. In a separate reaction, silica was carbonized at 550 °C under argon for 3 h in a tube furnace (Carbolite). The resulting BIS was ball milled for 5 min to give a fine homogeneous powder.

Silica nanospheres of 200 nm in size were made via the Stöber method.[14,15] 203 mL of ethanol (≥99.8%, VWR) and 15 mL of tetraethyl orthosilicate (TEOS) (Sigma-Aldrich, ≥99.0%) were mixed via magnetic stirring in a volumetric flask. After 10 min of mixing, 27 mL of deionized water was added, and following 10 min of mixing, 4 mL of ammonium hydroxide solution (VWR, 29%) was added dropwise to the solution. The solution was stirred for a further 24 h at 20 °C, followed by centrifugation at 5000 rpm for 15 min to separate the particles from the solution. The particles were rinsed with deionized water to remove excess ethanol, ammonium hydroxide, and TEOS, then centrifuged once more at 5000 rpm for 15 min, before being dried overnight at 80 °C.

BIS and Stöber silica were imaged using a FEI Inspect F scanning electron microscope (SEM) at an accelerating voltage of 5 kV.

### 2.2. Battery Cell Assembly

A 2.5 wt% solution of carboxymethyl cellulose (CMC) (Sigma) binder and deionized water was prepared. The desired solid amount of binder CMC 20 wt% in electrode was added to a Thinky mixer 10 mL pot. The conductive additive C-65 (MTI) 20 wt% in electrode was added and mixed at 1500 rpm for 5 min. Silica powder, 60 wt%, was added to the mixer and mixed together for a further 10 min to give a viscous ink. The ink was transferred to a 10 mL Perspex ball mill vial and milled in a Spex M8000 Mill with a stainless-steel bearing for 10 min. This ink was then applied to a carbon-coated copper foil (MTI) using a vacuum table (MTI) and doctor blade with thickness of 300 μm. The coating was air dried for 2 h and then placed in an 80 °C vacuum oven for a minimum of 6 h. The composition of working electrodes was: 60 wt% silica active material, 20 wt% conductive additive C-65, and 20 wt% CMC. Once dry, 12 mm diameter electrodes were punched from the foil and used for cell preparation. The mass loading of silica active material was 0.5–0.6 mg $cm^2$. Electrochemical experiments were performed using MIT2016-type coin cells with a Whatman glass fiber separator and lithium foil (Sigma-Aldrich) as the counter electrode. The electrolyte was 1 M $LiPF_6$ in a 1:1 solution of ethylene carbonate (EC) and dimethyl carbonate (DMC) (Sigma-Aldrich) with a 5 wt% fluoroethylene carbonate (FEC) additive (VWR). The cells were assembled in an argon filled glove box (MBraun) with oxygen and water contents less than 0.1 ppm. The charging rate was based on a theoretical capacity of 680 mAh $g^{-1}$ for silica. This theoretical capacity is based on the most commonly postulated reduction reaction ($2SiO_2 + 4Li \rightarrow Si + Li_4SiO_4$). The true theoretical capacity of silica materials cannot be determined without first knowing the reduction reaction mechanism.

ADVANCED
SCIENCE NEWS

www.advancedsciencenews.com

ADVANCED
ENERGY
MATERIALS

www.advenergymat.de

## 2.3. Potentiostatic Discharge (PSD)

The PSD was performed on a MACCOR 4000M Battery and Cell test system. The cells were first discharged galvanostatically at a rate of 0.1 C to 0.01 V. The cell was then subjected to 0.002 V potentiostatic discharge for 20 h. Following this, five constant current constant voltage (CCCV) cycles were performed at 0.1 C between 0.0 and 0.8 V. This PSD followed by five CCCV cycles was looped in accordance to the desired experiment, typically 20 loops, therefore 400 h total time at 0.002 V and 100 cycles.

## 2.4. Short-Circuit Reduction

Short-circuit reduction involved the application of a crocodile clip (RS-components) across the positive and negative electrodes of the 2016 coin cell, providing a path for current flow. The short-circuit was applied to freshly made half cells, unless stated otherwise. The short-circuited cells were sealed in a glass vial and placed within a temperature-controlled oven. The duration of short-circuiting and temperature of the oven were varied as specified in the Results section. Constant load discharge (CLD) was an equivalent experiment to short-circuit reduction but using a MACCOR 4000M Battery and Cell test system. Cells were cycled five times galvanostatically and then subjected to a constant load discharge of 0.8 Ω for the desired time duration. Cells could subsequently be cycled for capacity evaluation. All cycling experiments were performed in a temperature-controlled environment.

## 2.5. Electrochemical Impedance Spectroscopy (EIS) Measurement and Analysis

Electrochemical AC impedance experiments were performed on silica/lithium half-cells. The measurements were collected by a Solartron Modulab XM MTS, analyzing the frequency response between 0.01 and 100 000 Hz. Prior to impedance measurements, cells were held at open-circuit voltage (OCV) for 4 h to allow for sufficient voltage stabilization. Nyquist plots were fitted using ZView (Scribner and Associates).

## 2.6. Total Scattering, X-Ray Pair Distribution Function (X-PDF)

X-PDF data were collected on the I15-1 beamline at the Diamond Light Source UK, using an X-ray wavelength $\lambda = 0.161669$ Å ($E = 76.69$ keV). Electrode material samples were obtained by mechanical extraction from the copper current collector from post-mortem cells in an argon filled glovebox. The extracted material was then compacted into borosilicate glass capillaries of 1.17 mm (inner) diameter. Data from the samples, empty instrument, and empty capillary were collected, and integrated to 1D using DAWN.[16] Corrections for background, multiple scattering, container scattering, and attenuation were made, and the data were reduced to total scattering structure function, and Fourier transformed to the PDF, using the GudrunX software.[17]

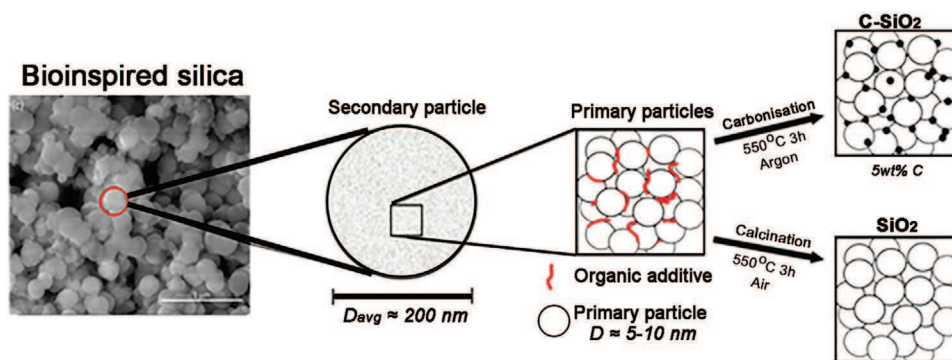## 3. Results and Discussion

### 3.1. Rate of Silica Reduction

#### 3.1.1. Potentiostatic Discharge

The reduction of silica within the electrode is a surface-driven process occurring at the interface between the silica particle and lithium-containing electrolyte. Therefore, increased surface area in contact with electrolyte may increase the rate of lithium reduction. For this reason, porous silica will likely provide better performance characteristics during electrochemical reduction. It has been shown previously (see Table S1, Supporting Information) that enhancing the electronic conductivity of silica by producing silica-carbon composites can increase the observed capacity. For both reasons BIS was chosen as the silica precursor in this study.

Previous reports have demonstrated the propagation of electrochemical reduction in silica by PSD.[2] Since the PSD treatment represents an additional processing step before silica electrodes can be incorporated into LIBs, it is desirable to assess new silica materials based upon the rate at which they react during PSD and the upper capacity they can achieve. To achieve this, we developed a new stepwise PSD, which allows for a quantitative measurement of both the capacity and the reduction time shown in **Figure 1**a. Initially, we used 200 nm
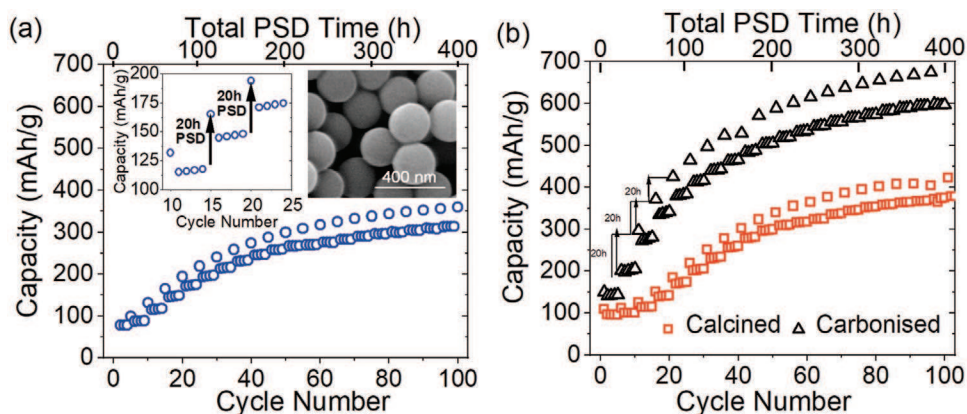


**Figure 1.** a) Capacity of 200 nm Stöber silica during 20 h PSD steps at 2 mV. Inset is a magnification of cycles 10–25 showing the increase in capacity after a 20 h PSD step. b) Capacity versus cycle life of BIS calcined (red) and carbonized (5 wt% carbon) (black).

2001826 (3 of 10)

**ADVANCED
SCIENCE NEWS**
www.advancedsciencenews.com

**ADVANCED
ENERGY
MATERIALS**
www.advenergymat.de

**Figure 2.** A schematic of bioinspired silica particle structure and theoretical representation of carbon coating and calcination to produce final product.[1]

Stöber silica (Figure 1a), as used by Lepoivre et al.[2] in order to provide a clear comparison to the BIS synthesized in this work. The stepwise PSD involved holding the electrode at the desired voltage for a determined period and then cycling five times reversibly to determine the capacity increase. In the case of Figure 1a, a 20 h PSD period was applied at 2 mV. The reduction can be studied at varying time resolutions by adjusting this step. The upper capacity of electrochemically reduced Stöber silica presented in Figure 1a was consistent with that reported by Lepoivre et al.[2] Of particular note is the first cycle of each step, which is consistently higher than the subsequent four cycles. This was due to a small amount of lithium deposition on the electrode, which is deposited during the low voltage PSD step (discussed further next).

In addition to its porous morphology, bioinspired synthesis provides another important attribute which can potentially address the low electronic conductivity of silica. Postsynthesis, an organic residue persists from the starting materials employed in the preparation of BIS, which is entrapped on the surface and within the silica structure. **Figure 2** presents a schematic of how the organic additives may be either calcined and completely removed by heating in air or can be carbonized by heating under an inert atmosphere. Surface area and pore volume analysis was used to confirm the formation of the carbonized structure, while thermogravimetric analysis showed the silica contained 5 wt% carbon after carbonization. SEM confirms no morphological differences between the uncalcined, calcined, and carbonized silica (Figure S1, Supporting Information).

The ability to electrochemically reduce calcined and carbonized BIS was assessed with the new stepwise PSD (see Figure 1b). A swifter capacity increase was observed for the carbonized BIS and after 400 h, a capacity of 600 mAh g$^{-1}$ was achieved. EIS was used to probe the contact resistance and charge transfer resistance, which were lower in the carbonized BIS electrode by 8.5% and 16.0%, respectively, compared to the calcined sample (Figure S2, Supporting Information). The increased conductivity of the carbon conducting layer on the silica increased the electronic accessibility of the reduction sites and thus increased the rate of electrochemical reduction. This first report of the use of a stepwise PSD showcases its power in interrogating the rate of electrochemical reduction.

The initial capacities of ≈90 mAh g$^{-1}$ observed in Figure 1 and Figure S3 (Supporting Information) before PSD are

attributed to the 20 wt% C-65 (carbon) which has a capacity of 241 mAh g$^{-1}$ (Figure S4, Supporting Information). In the absence of a PSD step, there was a minimal capacity increase over 100 galvanostatic cycles (Figure S3, Supporting Information). The small increase of 25 mAh g$^{-1}$ over 100 cycles for the carbonized BIS is attributed to a small amount of electrochemical reduction, which occurs during the low voltage stages of the galvanostatic cycling and is an indicator of the enhanced electrochemical reduction characteristics of the carbonized sample.
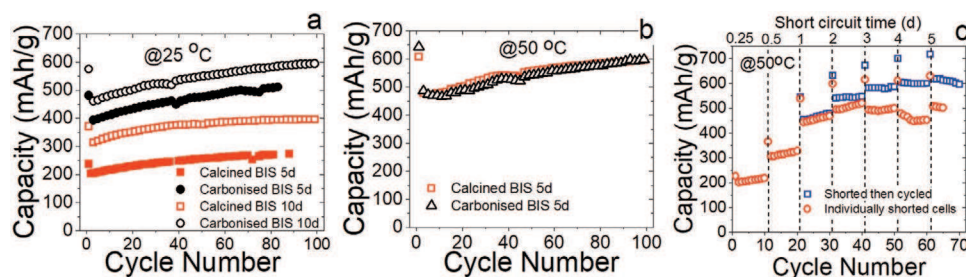
The stability of the reduced BIS electrodes was tested for 100 cycles following the pretreatment (see Figure S5, Supporting Information). The initial capacities for the carbonized and calcined electrodes were 625 and 410 mAh g$^{-1}$ respectively following a 400 h PSD. On galvanostatic cycling of these electrodes, it was found that there was minimal capacity fade with +2.4% and 0% change in capacity after 100 cycles respectively. The rate capabilities of calcined and carbonized BIS were tested between 0.1 and 5.0C using a theoretical capacity of 680 mAh g$^{-1}$. Both electrodes show excellent rate capabilities even at the high C-rate of 3.4 A g$^{-1}$ (Figure S6, Supporting Information), where the carbonized and calcined electrode can still provide 180 and 145 mAh g$^{-1}$ capacities, respectively. The return to stable capacity after the rate test indicates the stability of the reduced material and the robustness of the electrode fabrication.

### 3.1.2. Short-Circuit Electrochemical Reduction

According to the standard redox potentials of lithium and silica, the reduction of SiO$_2$ should be spontaneous with a potential of −2.13 V, following the process SiO$_2$ + 2Li → Si + 2Li$_2$O which describes the complete reduction of silica.

If an electronic pathway between the two electrodes is established, then due to the spontaneity of the reaction, this reduction reaction should proceed without any external bias. This reaction is here termed external short-circuiting and describes the connection of the positive electrode (silica) and the negative electrode (lithium) via a low resistance external circuit.

A series of silica-lithium half cells were externally short-circuited and left in a controlled temperature chamber before cycling (100 cycles, C/10) to study the effect of short-circuiting on the electrochemical reduction of silica. **Figure 3**a shows the capacity increase for calcined and carbonized silica following

**ADVANCED
SCIENCE NEWS**

www.advancedsciencenews.com

**ADVANCED
ENERGY
MATERIALS**

www.advenergymat.de

**Figure 3.** The results of galvanostatic cycling for 100 cycles after short-circuit treatment for 5 and 10 d. a) Short-circuit performed at 25 °C. b,c) Short-circuit performed at 50 °C.

either a 5 or 10 days short-circuiting period at 25 °C. The calcined silica electrodes reached capacities of 200 and 310 mAh g$^{-1}$ after 5 and 10 days, respectively, while the carbonized electrodes reached higher capacities of 395 and 460 mAh g$^{-1}$. After 100 cycles, the capacities of all four electrodes continued to increase further (discussed next). The rate of the reduction reaction, and hence the capacity achieved by the silica electrodes, were still improved by carbonization on the silica surface.

It is likely that the reduction reaction initially occurs at the silica interface with the lithium containing electrolyte, with the conversion of the center of the silica particles dependent on lithium diffusion into the bulk. Therefore, the reaction is limited by mass transfer with reduction becoming more and more restricted through the particle. The asymptotic behavior observed for the extent of reduction reaction during PSD, Figure 1, suggests that as the silica is increasingly reduced, it becomes harder for virgin material to react. We discuss this further in Section 3.3.

Solid-state diffusion of ions is strongly correlated with temperature which can overcome the activation energy barriers for hopping between sites. To promote mass transfer, cells were short-circuited at 50 °C for 5 d, then cycled (Figure 3b). The calcined and carbonized electrodes reached a capacity >490 mAh g$^{-1}$ in the second cycle and both rose to a capacity of 600 mAh g$^{-1}$ after 100 cycles. Both electrodes achieved higher overall capacities at this elevated temperature, supporting the idea of increased SiO$_2$ reduction at an elevated temperature. Both the calcined and carbonized electrodes reached the same capacity at the same rate, which suggests that at 50 °C, the electronic conductivity of the electrodes may no longer be a limiting factor for the rate of reduction. It is expected that higher temperatures still would increase the rate of electrochemical reduction. However, the cell cases used in this study were unable to hold at temperatures higher than 50 °C for prolonged periods.

In the short-circuiting experiment (Figure 3b), the highest initial capacities reached were ≈500 mAh g$^{-1}$, rising to ≈600 mAh g$^{-1}$ after 100 cycles. This is unlike the stepwise PSD where the 400 h pretreatment of the carbonized BIS produced a capacity of 600 mAh g$^{-1}$ which was then stable over 100 cycles. We attribute this to the cycling of the electrode during the stepwise PSD. The volume expansion of silicon during cycling has been widely reported[18] and the repeated cycling of the electrode during stepwise PSD allowed the electrode structure to evolve and achieve a stable 600 mAh g$^{-1}$ capacity. Differential capacity plots (Figure S7, Supporting Information) support this hypothesis, showing that the

established pathways for silicon lithiation/delithiation do not occur sequentially until the electrode is subjected to galvanostatic cycling. Figure 3c shows the results of an individual cell where the cycling was alternated with short-circuit steps to replicate the stepwise PSD procedure. The inclusion of periodic cycling resulted in a higher capacity than a static discharge process. The manipulation of the spontaneous reduction process removes the required energy to pretreat these cells, offering an appealing solution for large-scale fabrication.

## 3.2. Total Scattering Analysis of the Reduction Products from the Cell Pretreatment

Due to the amorphous nature of the products of silica reduction, previous studies have offered varied solutions to their nature. Silicon as a product has yet to be identified through direct characterization. The formation of amorphous silicon after lithiation is well documented in silicon-based active materials.[19] Here, the products of electrochemical reduction were characterized via total scattering X-ray PDF. PDF analysis includes scattering data from both the crystalline and amorphous components (i.e., both the Bragg peaks and the diffuse scattering), and so reveals structural information from materials where long-range order does not persist, as is the case for these reduction products.

Total scattering studies were performed on postmortem electrodes, with extreme care taken to prevent exposure to air or moisture. **Figure 4**a shows the X-PDF of the fresh composite electrode material (blue). Due to the composite nature of the electrodes, detailed characterization of control samples and polycrystalline silicon references were also required (Figure S12, Supporting Information). Since the as-studied sample contained both silica and carbon species, the resulting PDF contained peaks from both materials. Peak (**1**) at 1.60 Å (Si−O)[20] was the most prominent signal and is attributed to the Si−O atom–atom distance, confirming the presence of silica in the electrode, with a shoulder (peak **2**) at 1.42 Å (C−C)[21] due to the presence of carbon. The composite electrode has another peak **3** at 2.49 Å which is a combination of the carbon–carbon distance (2.46 Å)[21] from the CMC binder and conductive carbon additive employed and the O−O distance from silica (2.61 Å).[20] In addition, peak **4** at 2.92 Å in the composite material is formed of the 2.84 Å (C−C) peak from CMC binder and conductive carbon additive and the 3.06 Å Si−Si distance in silica.

**2001826 (5 of 10)**
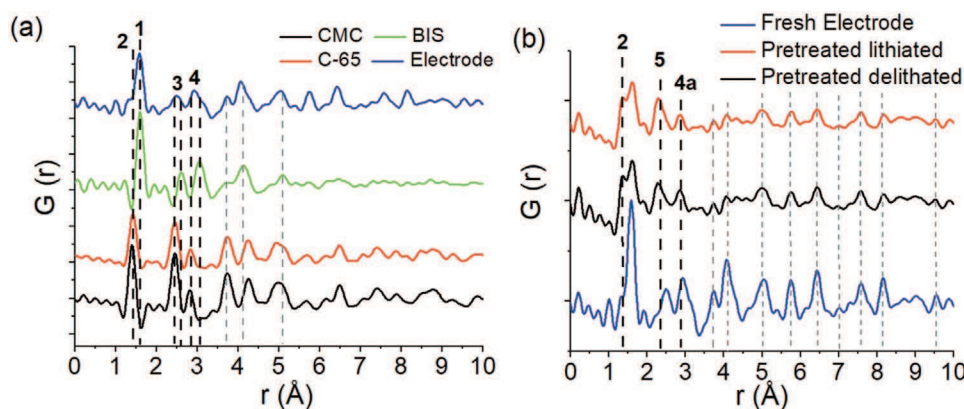
**Figure 4.** a) PDF of composite electrode and its individual components. Peaks corresponding to silica, binder, and conductive additive highlighted in dashed line. b) PDF of fresh electrode and after short-circuit at 50 °C for 20 h in both lithiated and delithiated state. Dotted line for peak-2 highlights the C—C bond distance (unaffected during reduction), while the lines for 4a and 5 highlight the main peak shifts observed during reaction.

The composite silica electrodes showed no Bragg peaks before or after electrochemical reduction. This was expected before reduction as each component of the electrode was amorphous in nature, and the lack of Bragg peaks in the reduced material shows no long-range order is present in the reduction products consistent with previous literature studies.[2,22–24] Figure 4b presents the PDF of the fresh silica electrode and the silica electrode after potentiostatic discharge (includes lithiated and delithiated states). As no changes occur to the carbon species during lithiation, the peak **2** for C—C (1.42 Å), invariant across this study, provides an internal standard. Note the areas and intensities of peaks in PDF measurements are complex and are not solely related to the abundance of the relative elements at a given distance. The relative ratios of peaks can be used in a qualitative manner to determine changes within the electrodes.

From Figure 4b, it is clear that relative to the carbon peak **2** at 1.42 Å, the peak attributed to the BIS (Si—O bond) at 1.60 Å reduced significantly after the PSD. Further, peak **4** at 2.92 Å shifted to 2.88 Å (peak **4a**). This is attributed to the loss of silica, leading to an increased contribution to this peak from the carbon signal at 2.84 Å (Figure S12, Supporting Information). Changes to both peak **2** and peak **4** strongly suggest the loss of silica, most likely by reduction to silicon. In addition, peak **5** at 2.35 Å appeared after the PSD and was present in the lithiated and delithiated states. This peak **5** at 2.35 Å matches with the control crystalline silicon samples measured in this study (Figure S12, Supporting Information) and with the well documented value for Si—Si bond distance.[25] Combining with the results from peaks **2** and **4a**, it is clear that silica was electrochemically reduced to amorphous silicon, which is present in the lithiated and delithiated material. These results provide the first direct evidence for the formation of elemental silicon in an amorphous state. This is further supported by the literature where it has been reported that silicon becomes amorphous after lithiation.[26] There are no additional peaks attributed to silicon, which suggest no long-range order.

The presence of Si—Si bonds at 2.35 Å in both the lithiated and delithiated state suggests that the highest lithiated state of silicon (cry-$Li_{3.75}Si$) was not reached. However, with the low electronic conductivity and relatively high current rates used for testing of these electrodes, the highest crystalline lithiated state cry-$Li_{3.75}Si$ may not form.[25,27,28] If all silicon is participating in lithiation during cycling, then lower lithiated states, such as those proposed by Grey and co-workers may form.[25] The presence of these structures in the lithiated samples would explain the presence of the Si—Si signal at 2.35 Å in the PDF. With regards to the lack of long-range order within the delithiated structure, the X-PDF results show the complete amorphization of the silicon domains formed during the electrochemical reduction. The absence of other clear signals in the PDF meant that other potential secondary reduction products ($Li_xSi_yO_z$/$LiO_x$ species) were not detected. As X-rays are insensitive to lighter elements such as Li, diffraction and scattering studies at a neutron source may be required to identify these elusive species.

### 3.3. Mechanism of Electrochemical Reduction in Silica Anodes

It has been shown above that increasing the temperature to 50 °C increased the rate of the electrochemical reduction of silica by lithium in short-circuit cells. **Figure 5**a shows that the same principle applies to the PSD method, with one 20 h potentiostatic discharge step at 2 mV increasing capacity to 500 mAh g^{−1} at 50 °C, compared to a negligible increase at 25 °C. Here, we can directly measure the current response through the process. By monitoring the current through the external circuit, one can record the number of electrons transferred and the rate of reduction. Figure 5b presents the current profile of cells at 25 and 50 °C during the first PSD step. The negative current corresponds to electrons flowing from the lithium to the silica electrode. The current response is small for the electrode at 25 °C, representing a lower electron transfer rate to the silica electrode. The maximum in the current profile for the electrode reduced at 50 °C is 35 times that at 25 °C (170 μA compared with 5 μA).

As the current is directly proportional to the rate of electrochemical reduction, the current profile can provide insight into the mechanism behind the reaction occurring. The current response is small during the first 20 h PSD for the
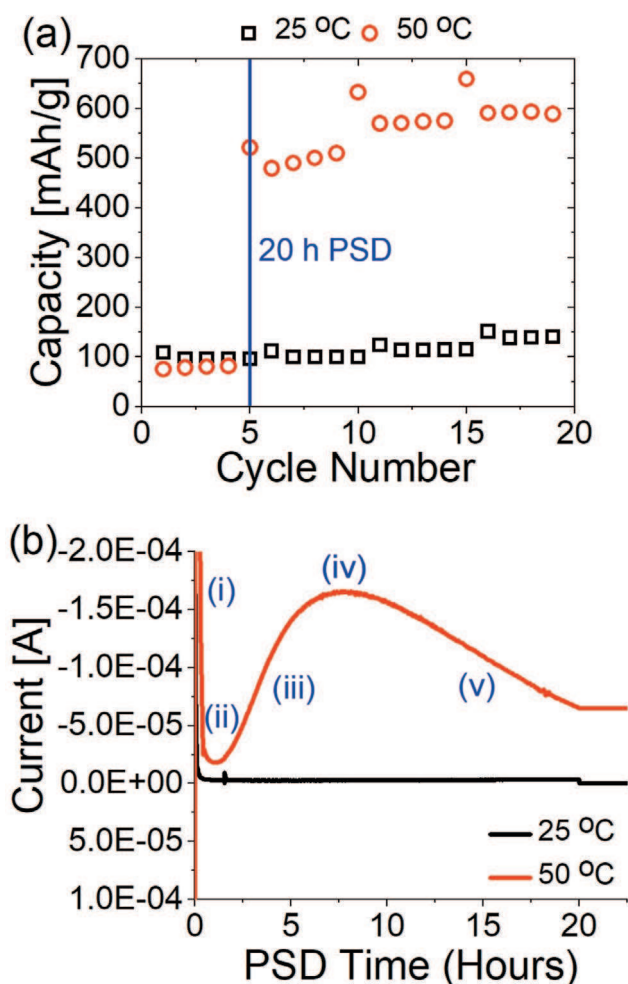
**Figure 5.** a) Capacity versus cycle life for BIS electrodes reduced with 20 h PSD steps at 50 °C (red) and at 25 °C (black). b) Current responses during the first PSD step.

electrode at 25 °C, representing slower electron transfer to the silica electrode. When comparing the shape of the current profiles for temperatures in Figure 5b and Figure S9 (Supporting Information), a clear pattern emerged (labeled **i–v**), as described next.

For the reduction at 50 °C, the current profile in Figure 5b clearly shows five distinct stages labeled (i–v):

i.  A spike in current as the charging regime is switched from a galvanostatic discharge at 0.1 C down to 50 mV to the PSD step at 2 mV. During this switch, the current spiked and then relaxed (0.5 h at 50 °C).
ii. This is followed by a minimum in current. A period where little current flowed between the two electrodes (0.5 to 1.5 h at 50 °C).
iii. A period with a relatively constant increase in current was observed (1.5 to 7.5 h at 50 °C).
iv. This increase in current reached a maximum in current, which corresponds to the highest rate of reduction (7.5 h at 50 °C).
v.  Finally, a period of gradual decrease in current at a relatively linear rate was observed (7.5 to 20 h at 50 °C).

Although different in magnitude and timescale, these features (**i–v**) can be assigned to the sample at 25 °C (Figure S9, Supporting Information). This is a strong indicator that the same chemical processes are occurring at both temperatures, but with differences in rates and extents.

With the aim of identifying the chemical processes occurring within the electrodes from stages i–v, EIS measurements were performed. **Figure 6**a highlights the important stages (**w–z**) where the impedance measurements were performed. Points **w**, **y**, and **z** represent measurements on the electrode, before PSD, and after PSD and then after ten galvanostatic cycles, respectively. Of particular relevance is the Nyquist plots in the lithiated state, which displays a single depressed semicircle feature at high frequencies followed by a sloping impedance to lower frequencies as seen in Figure 6b.[29]

Figure 6b presents the impedance frequency response of the lithiated electrode during the 20 h PSD treatment **x** in Figure 6a. The semicircle at high frequency can be fit with the equivalent circuit shown in Figure 6c, containing a parallel resistor and constant phase element (CPE). The electrode does not behave as an ideal capacitor (as expected), therefore a CPE was used to describe the capacitive nature of this element and account for real world behavior and the roughness of the active materials used.[29,30] Fitting the time-resolved impedance spectra allows for the extraction of the resistance of this element ($R_p$) and the CPE $p$ factor, where $p = 0$ is an ideal resistor and $p = 1$ describes an ideal capacitor and $Q_0$ is a constant (see Equation (1)). The value of $p$ was therefore used to determine the capacitive nature of a charge transfer process. Figure 6d shows a profile for the $p$ factor and the resistance of the electrode over 20 h of PSD. A rise in the resistance and the $p$ factor for the first 3 h was observed. The resistance began to decrease after 4 h and $p$ factor after 6 h. Both factors decrease in magnitude and level out by 13 h

$$Z_{CPE} = \frac{1}{Q_0 (j\omega)^p} \tag{1}$$

It is possible to correlate the capacitive and resistive nature of the electrode during the PSD (shown in Figure 6d) with the current profile features (i–v) shown in Figure 5b. Stage ii (a minimum in current flow) coincides when the $p$ and $R_p$ are at a maximum, leading to the slowest rate of reduction. This can be explained by charge build-up at the surface of the electrode due to the highest resistance, which hinders the electrochemical reduction reaction. We postulate that this charge build-up occurs as insufficient electron conduction pathways are available to facilitate the charge transfer reaction.

Stage iii is a period with a relatively constant increase in current up to a maximum. The beginning of this rise in current corresponds with the decrease in electrode resistance (Figure 6d). As silica gets reduced to silicon, and lithium silicates, these reduced species create new electron conduction pathways to adjacent virgin silica (note: the electronic conductivities of silicon, lithium silicates, and lithium oxides have been reported to be higher than insulating silica[31–33]). Therefore, as the reaction progresses, a positive feedback loop is created, where the rate of the reduction reaction continues to increase. The rapid decrease in the electrode resistance during stage iii directly supports this proposed hypothesis.

**2001826** (7 of 10)
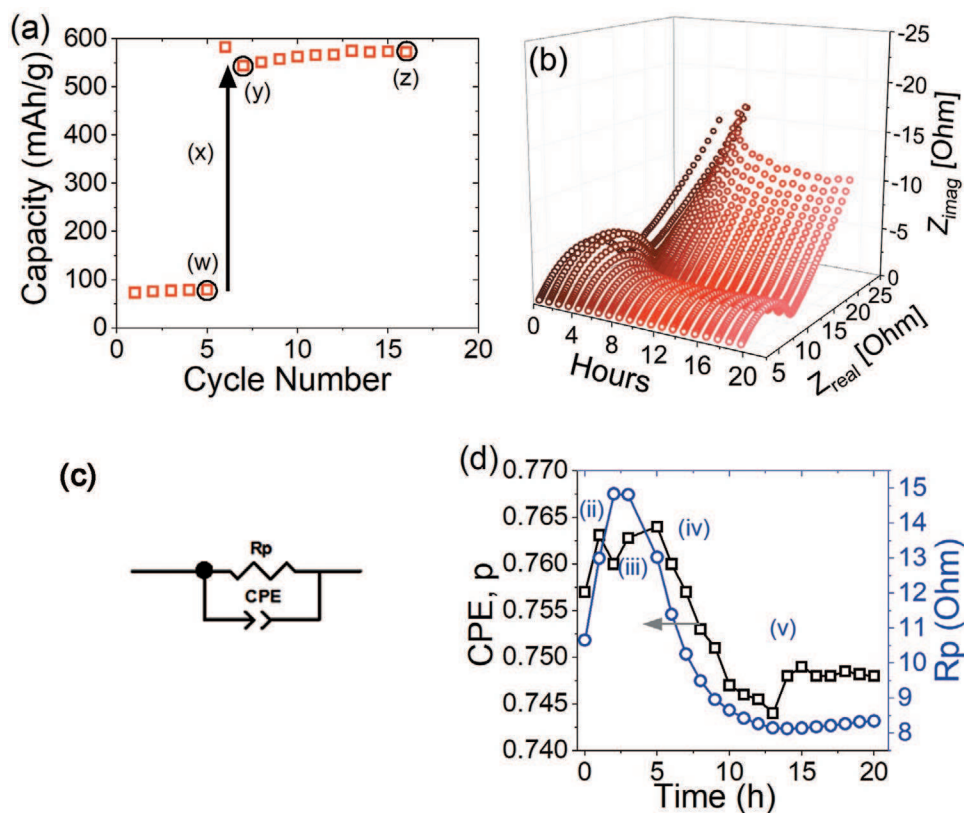
**Figure 6.** a) Capacity versus cycle life of a PSD reduced electrode at 50 °C, points (w–z) mark where electrochemical impedance measurements were performed. b) 3D Nyquist plot of the time-resolved impedance response throughout a 20 h PSD treatment at 50 °C, c) the resistance and CPE-P values for the equivalent circuit, d) fitted to the high frequency semicircular impedance response.

During stage iv, the maximum rate of reduction occurs. As the surface silica is reduced, the electronic conduction pathways are no longer the limiting factor for the rate of reaction. As a shell of reduced material is formed, the lithium diffusion pathways elongate and the process becomes limited by mass transfer. As the reduction front propagates into the particles in this manner, it is envisaged as a variation of a shrinking-core mechanism.
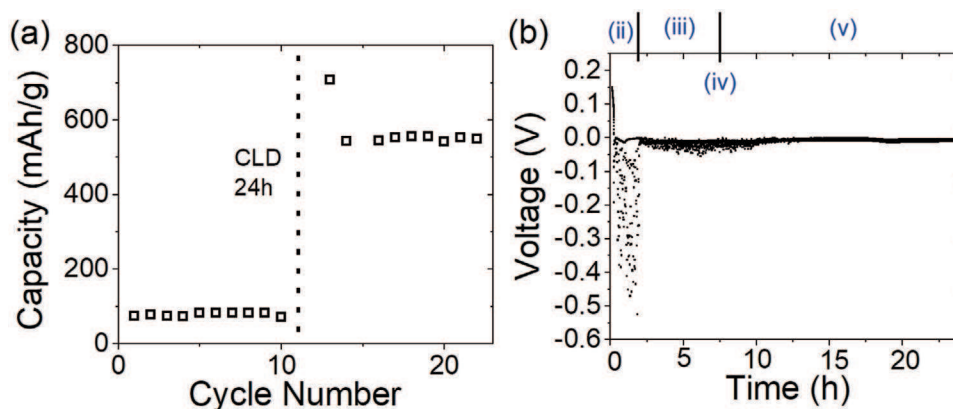
During stage ii, a charge build-up at the surface of the electrode occurs, thus hindering electrochemical reduction. The electrochemical reduction reaction is limited to those sites with sufficient electronic conduction pathways (i.e., those in contact with the conductive carbon network). To investigate this stage further, an experiment was designed to mimic the conditions of an external short-circuit discussed earlier. The use of a CLD is analogous to a short-circuit and can be performed on a galvanostat whilst simultaneously monitoring cell voltage and current. **Figure 7**a represents a cell after 24 h CLD at 50 °C, where a high and stable capacity of 550 mAh g$^{-1}$ can be reached. Unlike in PSD, the cell voltage may fluctuate and this can be monitored (Figure 7b). The reduction of silica via lithium is spontaneous during the short-circuit (constant load); however, fluctuation in the voltage will indicate the propensity of the reaction to occur.

The relationship of cell potential and Gibbs free energy is described by the variation of the Nernst theory in Equation (2),

where $z$ = number of electrons transferred, $F$ = the Faraday constant (C mol$^{-1}$), and $E_{cell}$ = cell potential difference (V)

$$\Delta G = -zFE_{cell} \tag{2}$$

According to Equation (2), for Gibbs free energy to be negative and hence a reaction to be spontaneous, the cell potential needs to be positive.[34] If the voltage across this lithium half-cell becomes negative, then this indicates lithium will no longer be transferred to the working electrode spontaneously. Figure 7b presents the voltage signal during the CLD: during stage ii, the voltage across the half-cell fluctuates between 0 and −0.6 V. As established earlier, during stage ii, little to no current flows across the cell, hence no reduction of silica is occurring. However, as Figure 7b shows, the potential at the electrode is changing significantly. We propose that during stage ii, lithium is deposited at the surface of the silica electrode and cannot react due to ineffective electron conduction pathways. This build-up of lithium and positive charge leads to the negative voltages in Figure 7b. A build-up of charge during this period also corresponds with the increased capacitance detected during stage ii as measured by EIS (Figure 6d). As the reduction reaction progresses, initially from sites with established electronic conduction pathways, the reduced product becomes more electronically conducting, thus providing further sites for the reduction reaction to occur at a faster rate (stage iii).

**ADVANCED
SCIENCE NEWS**

www.advancedsciencenews.com

**ADVANCED
ENERGY
MATERIALS**

www.advenergymat.de

**Figure 7.** a) Capacity profile of a BIS electrode before and after 24 h of a constant load discharge (CLD) of 0.8 Ω at 50 °C. b) Voltage signal during the 24 h CLD step.

As the current begins to rise, stage iii, and throughout stages iv and v, the voltage fluctuates only slightly between 0 and −0.05 V. After 13 h of CLD, the voltage shows no fluctuations. The small fluctuations in cell voltage observed during stages iii, iv, and v perhaps indicate that some lithium build-up on the surface still occurs during these stages but to a lesser extent as the surface of the silica particles may not have been entirely reduced at these stages. We suggest that as electronic conduction pathways progress to these sites, a voltage drop will occur as a small quantity of lithium deposits. This may be related to the porous nature of the silica particles: Pores within the particle have no way of contacting the conductive carbon network, they may however be wetted by lithium-containing electrolyte. These voltage signals could be a result of the reduction reaction front penetrating deeper into the particles and as such establishing electronic conduction pathways to these pore sites which are in contact with electrolyte. The exact nature of the negative potentials measured in stage iii is much smaller than the large negative voltage signals seen in stage ii. However, both fit with a model of reduced material providing conduction pathways to virgin silica sites, with the reaction progressing with a shrinking core like mechanism of reduction within the particles. Combining the results discussed above, **Figure 8** presents a schematic overview of the proposed electrochemical reduction at the level of a single BIS particle.
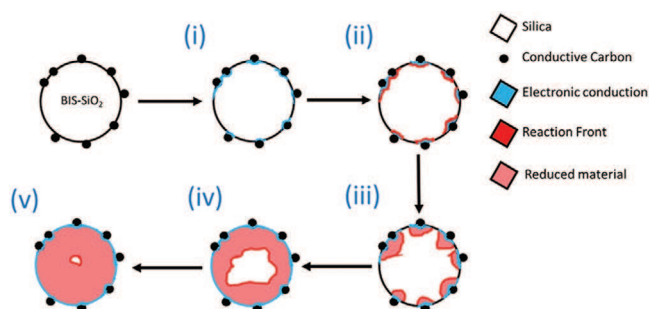
The voltage profile in Figure 7b indicates that the majority of the electrochemical reduction has occurred after 13 h. Performing CLD on a fresh cell for 13 h at 50 °C resulted in a capacity of 500 mAh g$^{-1}$, with a stable capacity of 600 mAh g$^{-1}$ reached after 20 cycles. The coulombic efficiency was 90% rising to 99% after 20 cycles. This represents a significant decrease in the electrochemical reduction time needed to produce high and stable capacities from 250 h required to reduce Stöber silica particles with capacity of 400 mAh g$^{-1}$,[2] to 13 h reported here. The high capacity and stable cycle life demonstrate the enormous potential for the use of BIS as an anode material.

## 4. Conclusion

This study puts forward a new method to utilize bioinspired silica particles for application as silica-based anodes in lithium-ion batteries. Compared to anode grade silicon, silica as a low-cost material is a sustainable source given its abundance, hence its direct use can clearly help meet the economic targets. We have demonstrated that the reduction reaction proceeds via a shrinking core-like mechanism as conductive pathways progress into the silica particles during the reduction. The reduction products are amorphous in nature, however, through the use of total scattering X-ray pair distribution analysis, we have directly observed the formation of electrochemically reduced silicon for the first time. By establishing a new pretreatment protocol, to reduce the silica particles at an elevated temperature, we can significantly reduce the pretreatment time required to 13 h compared with previous literature values of 100s of hours,[2] offering significant commercial advantages.[2,35] The bioinspired silica anodes could provide a stable high capacity of 635 mAh g$^{-1}$ after 100 cycles which is significantly higher than that of graphite (372 mAh g$^{-1}$). Further work includes a detailed study of the current profile during the electrochemical reduction of silica in order to understand and optimize the reduction kinetics. Characterization of the lithium-containing intermediate reduction species and the morphology of the Si/SiO$_x$ will be valuable in future studies using advanced techniques such as neutron total scattering and operando spectroscopic and



**Figure 8.** Graphical representation of the mechanism for the electrochemical reduction of BIS at a particle level. i–v correspond to stages shown in Figure 5b.

microscopic methods. As some silicon chemistries currently in use for LIBs contain varying amounts of silica within their structure, whether as an impurity or a passivating layer, the results presented here should aid in understanding behavior in other silica-containing systems, providing significant ramifications for these materials beyond their use as an active anode material.

## Supporting Information

Supporting Information is available from the Wiley Online Library or from the author.

## Conflict of Interest

The authors declare no conflict of interest.

[1] M. M. Thackeray, C. Wolverton, E. D. Isaacs, *Energy Environ. Sci.* **2012**, *5*, 7854.
[2] F. Lepoivre, D. Larcher, J. Tarascon, *J. Electrochem. Soc.* **2016**, *163*, A2791.
[3] M. Pagliaro, *Silica-Based Materials for Advanced Chemical Applications*, Royal Society of Chemistry, London **2009**.
[4] Z. Liu, Q. Yu, Y. Zhao, R. He, M. Xu, S. Feng, S. Li, L. Zhou, L. Mai, *Chem. Soc. Rev.* **2019**, *48*, 285.
[5] H. J. Kim, S. Choi, S. J. Lee, M. W. Seo, J. G. Lee, E. Deniz, Y. J. Lee, E. K. Kim, J. W. Choi, *Nano Lett.* **2016**, *16*, 282.
[6] T. Tan, P. K. Lee, D. Y. W. Yu, *J. Electrochem. Soc.* **2019**, *166*, A5210.
[7] B. Guo, J. Shu, Z. Wang, H. Yang, L. Shi, Y. Liu, L. Chen, *Electrochem. Commun.* **2008**, *10*, 1876.
[8] A. Lisowska-oleksiak, A. P. Nowak, B. Wicikowska, *RSC Adv.* **2014**, *4*, 40439.
[9] W.-S. Chang, C.-M. Park, J.-H. Kim, Y.-U. Kim, G. Jeongc, H.-J. Sohn, *Energy Environ. Sci.* **2012**, *5*, 6895.
[10] C. Drummond, R. McCann, S. V. Patwardhan, *Chem. Eng. J.* **2014**, *244*, 483.
[11] S. V. Patwardhan, *Chem. Commun.* **2011**, *47*, 7567.
[12] S. V. Patwardhan, S. S. Staniland, *Green Nanomaterials*, IOP, Bristol, UK **2020**.
[13] J. R. H. Manning, E. Routoula, S. V. Patwardhan, *JoVE* **2018**, e57730.
[14] G. H. Bogush, M. A. Tracy, C. F. Zukoski, *Colloids Surf.* **1988**, *34*, 81.
[15] Y. Takeuchi, *J. Phys. Ther. Sci.* **2017**, *29*, 112.
[16] J. Filik, A. W. Ashton, P. C. Y. Chang, P. A. Chater, S. J. Day, M. Drakopoulos, M. W. Gerring, M. L. Hart, O. V. Magdysyuk, S. Michalik, A. Smith, C. C. Tang, N. J. Terrill, M. T. Wharmby, H. J. Wilhelm, *Appl. Cryst.* **2017**, *50*, 959.
[17] A. K. Soper, E. R. Barney, *J. Appl. Crystallogr.* **2011**, *44*, 714.
[18] M. K. Y. Chan, C. Wolverton, J. P. Greeley, *J. Am. Chem. Soc.* **2012**, *134*, 14362.
[19] M. T. McDowell, S. W. Lee, W. D. Nix, Y. Cui, *Adv. Mater.* **2013**, *25*, 4966.
[20] A. C. Wright, *J. Non-Cryst. Solids* **1990**, *123*, 129.
[21] F. Li, J. S. Lannin, *Phys. Rev. Lett.* **1990**, *65*, 1905.
[22] J. Tu, Y. Yuan, P. Zhan, H. Jiao, X. Wang, H. Zhu, S. Jiao, *J. Phys. Chem. C* **2014**, *118*, 7357.
[23] X. Cao, X. Chuan, S. Li, D. Huang, G. Cao, *Part. Part. Syst. Charact.* **2016**, *33*, 110.
[24] Y. Yao, J. Zhang, L. Xue, T. Huang, A. Yu, *J. Power Sources* **2011**, *196*, 10240.
[25] B. Key, M. Morcrette, J. Tarascon, C. P. Grey, *J. Am. Chem. Soc.* **2011**, *133*, 503.
[26] J. Li, J. R. Dahn, *J. Electrochem. Soc.* **2007**, *154*, A156.
[27] K. Ogata, E. Salager, C. J. Kerr, A. E. Fraser, C. Ducati, A. J. Morris, S. Hofmann, C. P. Grey, *Nat. Commun.* **2014**, *5*, 3217.
[28] V. L. Chevrier, J. W. Zwanziger, J. R. Dahn, *J. Alloys Compd.* **2010**, *496*, 25.
[29] ZView, Scribner Associates, Inc., **2016**.
[30] W. H. Molder, J. H. Sluyters, *J. Electroanal. Chem. Interfacial Electrochem.* **1990**, *285*, 103.
[31] W. R. H. John, *J. Solid State Chem.* **1981**, *278*, 271.
[32] I. M. Hodge, M. D. Ingram, A. R. West, *J. Am. Ceram. Soc.* **1976**, *59*, 360.
[33] K. Zhao, G. A. Tritsaris, M. Pharr, W. L. Wang, O. Okeke, Z. Suo, J. J. Vlassak, E. Kaxiras, *Nano Lett.* **2012**, *12*, 4397.
[34] A. Bard, L. Faulkner, *Electrochemical Methods: Fundamentals and Applications*, Wiley, New York **1980**.
[35] A. N. Norberg, N. P. Wagner, H. Kaland, F. Vullum-Bruer, A. M. Svensson, *RSC Adv.* **2019**, *9*, 41228.